International Journal of Signal Processing, Image Processing and Pattern Recognition
Vol.9, No.8 (2016), pp.87-96
http://dx.doi.org/10.14257/ijsip.2016.9.8.07

Comparison of Robust Methods for Shear Wave Speed Estimation by Simulation

Hao Yin[1*], Dong C. Liu[2] and Xin Liu[3]

School of Computer Science, Sichuan University, No.24 South Section 1, 1st Ring Road, 610065 Chengdu, China
[1]yinhao@scu.edu.cn, [2]dongcliu@163.com

Abstract

Mechanical properties of tissue are often related to the pathological state of tissue. Therefore, non-invasively measuring tissue stiffness has important clinical applications. With the assumption of isotropy, incompressibility and linearity, the shear modulus of tissue is related to its shear wave propagation speed. Acoustic radiation force from a focused ultrasound beam can be used to generate shear waves at the focal region within tissue, which propagate orthogonally to the direction of the pushing ultrasound beam. The shear wave speed can be estimated based on the so called time-to-flight principle. The shear wave arrival time determined at several lateral positions along the shear wave propagation path can be measured by the displacement profiles, which can be tracked using correlation-based method by pulse-echo ultrasound. This approach has been successively used with various modifications by several groups. The purpose of this study is to design a simulation method to generate the pulse-echo ultrasound signal, calculate the displacement profile in the spatial and time domain, and estimate the shear wave speed using RANSAC, Radon Sum and robust linear regression method, compare and analyze the algorithm performance of these methods.

Keywords*: medical ultrasound, simulation, shear wave speed, RANSAC, Radon Sum, robust linear regression*

1. Introduction

Mechanical properties of tissue are often related to the pathological state of tissue. Therefore, non-invasively measuring tissue stiffness has important clinical applications. With the assumption of isotropy, incompressibility and linearity, the shear modulus of tissue is related to its shear wave propagation speed. Acoustic radiation force from a focused ultrasound beam can be used to generate shear waves at the focal region within tissue, which propagate orthogonally to the direction of the pushing ultrasound beam [1-2]. The shear wave speed can be estimated based on the so called time-to-flight principle. The shear wave arrival time determined at several lateral positions along the shear wave propagation path can be measured by the displacement profiles, which can be tracked using correlation-based method by pulse-echo ultrasound. This approach has been successively used with various modifications by several groups [3-5].

The purpose of this study is to design a simulation method to generate the pulse-echo ultrasound signal, calculate the displacement profile in the spatial and time domain, estimate the shear wave speed using Random Sample Consensus (RANSAC) [11], Radon Sum [13] and robust linear regression method, and analyze the performance of these methods.

* Corresponding Author

ISSN: 2005-4254 IJSIP

2. Computer Simulation

2.1. Displacement Field

Bercoff provided an analytical expression of the Green's function in an infinite viscoelastic soft solid [6]. It takes into account shear, bulk, and coupling waves in viscoelastic media so that 3D simulations derived from this Green's function allows the precise modeling of the transient propagation of shear waves in soft tissues activated by ultrasonic focused beams. The analytical solution of the Green's function is given below, which is the starting point of a 3D simulation.

$$g_{zz}(\vec{r},t) = g_{zz}^{p}(\vec{r},t) + g_{zz}^{s}(\vec{r},t) + g_{zz}^{ps}(\vec{r},t) \tag{1}$$

The first term g_{zz}^{p} represents the pure bulk component. The second term g_{zz}^{s} corresponds to the pure shear component. The third term g_{zz}^{ps} is a coupling term between bulk and shear waves. In the three-dimensional (3D) simulation, only the displacement field in the depth direction z is considered. The propagation direction of the shear wave is the horizontal direction x.

$$g_{zz}^{p}(r,t) = \frac{1}{4\pi\rho c_p}\frac{1}{\sqrt{2\pi v_p t}}\gamma_3\gamma_3\frac{1}{r}e^{-\frac{\left(t-\frac{r}{c_p}\right)^2 c_p^2}{2v_p t}} \tag{2}$$

$$g_{zz}^{s}(r,t) = \frac{1}{4\pi\rho c_s}\frac{1}{\sqrt{2\pi v_s t}}\frac{1-\gamma_3\gamma_3}{r}e^{-\frac{\left(t-\frac{r}{c_s}\right)^2 c_s^2}{2v_s t}}$$

$$g_{zz}^{ps}(r,t) = -\frac{1}{4\pi\rho}(3\gamma_3\gamma_3-1)\frac{1}{r^3}\left(I_p(r,t)+I_s(r,t)\right)$$

$$I_p(r,t) = \frac{\sqrt{v_p t}}{\sqrt{2\pi}c_p}\left[e^{-\frac{t^2c_p^2}{2v_p t}} - e^{-\frac{\left(t-\frac{r}{c_p}\right)^2 c_p^2}{2v_p t}}\right] + \frac{t}{2}\left[Erf\left(\frac{c_p t}{2v_p t}\right) - Erf\left(\frac{c_p\left(t-\frac{r}{c_p}\right)}{2v_p t}\right)\right]$$

$$I_s(r,t) = \frac{\sqrt{v_s t}}{\sqrt{2\pi}c_s}\left[e^{-\frac{t^2c_s^2}{2v_s t}} - e^{-\frac{\left(t-\frac{r}{c_s}\right)^2 c_s^2}{2v_s t}}\right] + \frac{t}{2}\left[Erf\left(\frac{c_s t}{2v_s t}\right) - Erf\left(\frac{c_s\left(t-\frac{r}{c_s}\right)}{2v_s t}\right)\right]$$

The modulus r located at coordinate (x,y,z) is given by $\mathrm{r} = \sqrt{x^2+y^2+z^2}$, the component of the corresponding unitary vector $\gamma_3 = z/r$. The symbols ρ, c_p, c_s, v_p, v_s depict density, the velocity of the compressional wave, the velocity of the shear wave, kinematic bulk viscosity, and kinematic shear viscosity respectively.

2.2. Scatter Field

In medical ultrasound imaging, the backscatter signal results from acoustic insonification of a collection of scatterers. The density of the scatterers is specified as scatterers per resolution cell. To achieve fully developed speckle demonstrated by Palmeri [7], at least 11 scatterers/resolution cell was necessary in the presented simulation. The scatterers in the artificial phantom were generated with uniformly distributed position

within $20 \times 5 \times 10$ mm cube. Each scatter was assigned with a Gaussian distributed amplitude.

The devised scatter ROI contains a point-like source excitation located at point $\overrightarrow{r_0}\ (x,y,z) = (0,0,0)$, which emits a temporal delta function. The displacement field induced by this point source corresponds to the solution of the Green's function based on Eq. (1, 2). The medium parameters chosen for this simulation were $\rho = 1000\ kg/m^3$, $c_p = 1540\ m/s$, $c_s = 2\ m/s$, $\eta_p = 0Pa.s$, $\eta_s = 0.2Pa.s$. The bulk and shear viscosity η_p and η_s determine the kinematic bulk and shear viscosity $v_p = (\eta_p + 2\eta_s)/\rho$ and $v_s = \eta_s/\rho$ respectively. The temporal interval t elapsed from 0.1 to 25 milliseconds with pulse repetition frequency (PRF) 5 kHz. Time zero is a singularity for Equation (2), so the simulation started from $0.1ms$.

When the scatter ROI was placed in the transducer coordinate system, the ROI was translated -5mm in horizontal direction *x* and 30mm in depth direction *z*. The 2D coordinate system is presented in Figure 1.

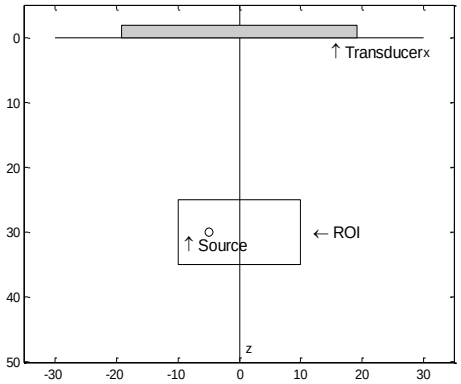

Figure 1. 2D Transducer Coordinate System

The pulse echoes were simulated by using Field II [8]. A 128 elements linear array transducer with 64 active elements was used. Hanning apodization was used for active elements in transmit and receive. The element height was 5mm, the pitch was 0.3mm. The range of the scatter ROI in the depth direction was 10mm, so only a single transmit and receive focus was placed at 30 mm from the transducer surface. The center frequency f_c, sampling frequency f_s and PRF f_{prf} were 5 MHz, 40 MHz and 5 kHz respectively. The displacement field calculated before were normalized with the amplitude 20 nm so as to match the localized micron-scale displacement induced by radiation force. The field simulation was performed with 9 scan lines ranged from -4 to 0 mm separated by 0.5mm in lateral direction in the 2D transducer coordinate system.

2.3. Displacement Estimation

The frequency domain technology, cross spectrum method [9] was used to calculate the axial displacement. If the received RF echo and its frequency spectrum are expressed as *s*(*t*) and *S*(*f*) respectively, the cross spectrum of the pre-compression (*s*0) and post-compression (*s*1) signals can be calculated as:

$$S_0^*(f)S_1(f) = \left|S(f)\right|^2 e^{-j2\pi f(\tau_1-\tau_0)} \tag{3}$$

where τ_0 and τ_1 are the time delays respectively. The gate size for the localized window was 1mm. The change in time delay corresponds to the displacement, which can be estimated from the phase of the cross spectrum.

$$\Delta\theta(f) = -2\pi f(\tau_1 - \tau_0), u = \frac{c}{2}\frac{\Delta\theta(f)}{\omega_c}|_{f=f_0} \quad (4)$$

The center frequency f_0 was estimated by finding the frequency at which the maximum occurs in the cross spectrum. The estimated displacement profiles at several lateral positions were depicted in Figure 2. In the displacement vs. time curves, the peak displacement propagates along horizontal direction away from the excitation region located at *x=-5mm* in the transducer coordinate system as shown in Figure 1.

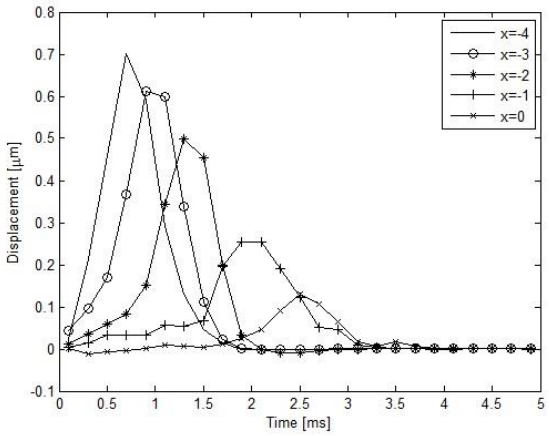

Figure 2. Displacement Profiles

3. Estimation of Shear Wave Speed

The estimation of shear wave speed can be calculated using time-to-peak (TTP) approach [10] under the assumption that a linear relationship exists between the lateral positions and the corresponding arrival times of the peak displacement.

The TTP values were extracted over a 2D ROI both in lateral and depth dimensions. A linear model which fits the variation of TTP values over this spatial domain was given below:

$$\boldsymbol{x} = p_1 + p_2\boldsymbol{t} + p_3\boldsymbol{z} \quad (5)$$

where $\boldsymbol{x}, \boldsymbol{z}, \boldsymbol{t}$ are vectors of lateral, depth and TTP values respectively, and $\boldsymbol{p} = [p_1, p_2, p_3]$ is the unknown model parameter vector. The component p_2 corresponds to the estimated shear wave speed. In the proposed simulation, 5 lateral positions and 5 depth position ($\mathrm{z} = 28,29,30,31,32\mathrm{mm}$) totally 25 TTP values were selected.

(RANSAC) is a widely used iterative method to estimate parameters of a mathematical model from a set of observed data which contains outliers [11]. Wang have applied the RANSAC method to the problem of shear wave speed estimation from the ultrasonically tracked displacement profiles [12]. The minimal sample set required to fit a plane is three. Therefore, three points were randomly selected to solve equation (5) as a trial solution. Then, points matching this trial estimate within the expected measurement error were identified as inliers, while others were outliers. The best fit would be kept as the estimated solution after iteration.

Rouze proposed the Radon Sum transformation method for estimation of shear wave speed [13]. The shear wave propagation was characterized by the trajectory of the peak displacement and time. Like the Radon transform, a linear model was considered to calculate the sum of displacement $d(x,t)$ along the trajectory from a starting position

(x_{start}, t_{start}) to an ending position (x_{end}, t_{end}), which could be used as a metric to characterize the wave motion. In order to increase the temporal resolution of the peak displacement times, the displacement profiles need to be up-sampled to a frequency of 100 kHz.

$$\frac{x - x_{start}}{t - t_{start}} = \frac{x_{start} - x_{end}}{t_{start} - t_{end}} \tag{6}$$

$$S(t_{start}, t_{end}) = \sum_{x_{start}}^{x_{end}} d(x, t)$$

Iteratively reweighted least squares (IRLS) [14] was used as a robust linear regression method to compare the results of RANSAC and Radon Sum methods. Standard deviation (SD) was estimated by median absolute deviation (MAD) method which is a robust alternative to SD. The residuals were adjusted using leverages, which correspond to the diagonal elements of the hat matrix. Tukey bisquare function was used to compute the weights, which will be small if the standardized residuals are large and thus down weight the effects of outliers.

$$\boldsymbol{p}^k = \left[X^T W^{(k-1)} X\right]^{-1} X^T W^{(k-1)} \boldsymbol{y} \tag{7}$$

where k is the number of iteration, $\boldsymbol{p}$ is the parameter vector, W is the weight matrix, $X = [\mathbf{1}\ \mathrm{t}\ \boldsymbol{z}]$ is the matrix of TTP values and depth coordinates, and $\boldsymbol{y} = \boldsymbol{x}$ is the vector of lateral coordinates, as expressed in Eq. (5).

4. Results and Discussion

The synthetic TTP values calculated through the Green's function, Field II simulation and cross spectrum estimation would not match up with the theoretical shear wave speed, in other words, the data set contains outliers. Both RANSAC and IRLS methods use a mathematical model to express the relationships among lateral positions, TTP values and depth positions. The parameters can be estimated by fitting the observed data with the plane model even when outliers are present in the data set (Figure 3(a) and 3(c)). The Radon Sum image was shown in Figure 3(b), the optimal trajectory is identified by the peak Radon sum indicated as the brightest point in the image.

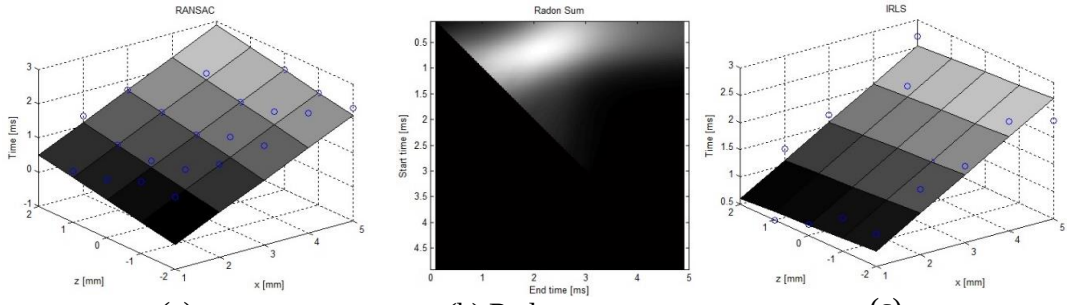

(a) (b) Radon sum (c)

Figure 3. Results of Three Methods

The displacement profiles were first obtained using 22 scatterers per cubic millimeter, shear wave speed 2m/s and gate size 1mm mentioned in cross spectrum method. Considering the computation time of simulation, there were totally 10 independent simulation for this configuration. The results of the estimated shear wave speed are listed in Table 1 using the methods aforementioned with different signal-to-noise (SNR) values from 10 to 60 dB. The mean value and standard deviation (SD) of speed are depicted by μ

and σ respectively, while bias is calculated by $100\% \times |\mu - c_s|/c_s$. Figure 4 shows the same results in bar graph. The bar values are the mean values of the estimated shear wave speed, while the error bars depict the standard derivation.

The results indicate that Random Sum method and IRLS method are not so sensitive to SNR compared with RANSAC method, and the values of SD are smaller. While the estimated values of shear wave speed by RANSAC method and IRLS method are closer to the real value than Radon Sum method, the values of bias are smaller.

Both RANSAC and IRLS are iterative methods to estimate the shear wave speed. In each iteration, RANSAC algorithm randomly selects a trial solution without using the knowledge from the previous iterations. So repeated executions of RANSAC on the same displacement profiles can yield varying values. In each step of the IRLS method, the weights will be updated based on the previous trial solution. Hence it is more stable than RANSAC.

For the Radon Sum method, an outlier can only contribute to the Radon sums through that point, not affect the sums for trajectories near the optimal trajectory. However, the displacement profiles need to be up-sampled to a frequency of 100 kHz to increase the temporal resolution of the peak displacement times.

Table 1. Results of Estimated Shear Wave Speed
($c_s = 2m/s$, $density = 22\ scatters/mm^3$)

SNR	IRLS		RANSAC		Radon Sum	
	$\mu \pm \sigma$	bias	$\mu \pm \sigma$	bias	$\mu \pm \sigma$	bias
10 dB	2.0172±0.1952	0.86 %	1.9896±0.2962	0.52 %	2.2730±0.4673	13.65 %
20 dB	2.0646±0.1596	3.23 %	1.9461±0.2367	2.69 %	2.1213±0.1512	6.07 %
30 dB	2.0393±0.1683	1.96 %	1.8745±0.2155	6.27 %	2.1084±0.1461	5.42 %
40 dB	2.0463±0.1688	2.32 %	2.0629±0.3248	3.14 %	2.1064±0.1480	5.32 %
50 dB	2.0439±0.1709	2.19 %	2.0368±0.2865	1.84 %	2.1064±0.1480	5.32 %
60 dB	2.0198±0.1614	0.99 %	1.9382±0.2736	3.09 %	2.1064±0.1480	5.32 %

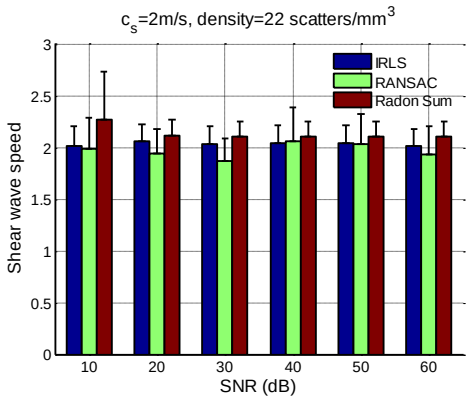

Figure 4. Results with Different SNR

The scatterers in the artificial phantom were generated as fully developed speckle with at least 11 scatter/resolution cell. The experiments were carried out with different scatter

density, 11, 22, 33 scatterers/mm^3. Since the volume of the resolution cell at 5MHz central frequency is about 1.45 cubic millimeter, all of the scatter density values satisfy the constraint condition. The number of independent simulation is also 10 for each scatter density configuration. The results of the estimated shear wave speed with different scatter density values are listed in Table 2 and shown in Figure 5.

Table 2. Results of Estimated Shear Wave Speed with Different Scatter Density ($c_s = 2m/s, SNR = 30dB$)

Scatter density	IRLS		RANSAC		Radon Sum	
	$\mu \pm \sigma$	bias	$\mu \pm \sigma$	bias	$\mu \pm \sigma$	bias
11	2.0615±0.1224	3.07 %	2.0265±0.3142	1.32 %	2.2915±0.2867	14.57 %
22	2.0393±0.1683	1.96 %	1.8745±0.2155	6.27 %	2.1084±0.1461	5.42 %
33	2.0792±0.1269	3.96 %	2.0713±0.3197	3.57 %	2.1541±0.1589	7.70 %

The scatter density has limit effect on RANSAC and IRLS methods. When the scatter density takes a lower value, such as 11, the significant change for Radon Sum method comes from the gross outliers. The number of samples in the spatial domain data set is limited so that the gross outliers will remarkably influence the result of calculation. That's the reason that the estimated values of Radon Sum method diverge from the real value much more than those of RANSAC and IRLS method.

The estimated values of shear wave speed with different theoretical speed values are listed in Table 3 and shown in Figure 6. There are also 10 independent simulations for each shear wave speed. IRLS method remains advantage over the other two methods in terms of bias and SD.

Table 3. Results of Estimated Shear Wave Speed with Different Real Values ($density = 22\ scatters/mm^3, SNR = 30dB$)

Shear Wave Speed (m/s)	IRLS		RANSAC		Radon Sum	
	$\mu \pm \sigma$	bias	$\mu \pm \sigma$	bias	$\mu \pm \sigma$	bias
1	1.0257±0.0430	2.57 %	0.9973±0.1305	0.27 %	1.1188±0.0777	11.88 %
2	2.0393±0.1683	1.96 %	1.8745±0.2155	6.27 %	2.1084±0.1461	5.42 %
3	3.1194±0.2198	3.98 %	3.1951±0.4444	6.50 %	3.2741±0.2472	9.14 %
4	4.0628±0.1921	1.57 %	4.2250±0.5458	5.62 %	4.2739±0.4129	6.85 %

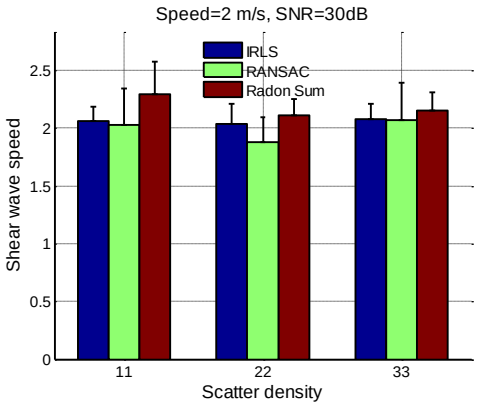

Figure 5. Results with Different Scatter Density

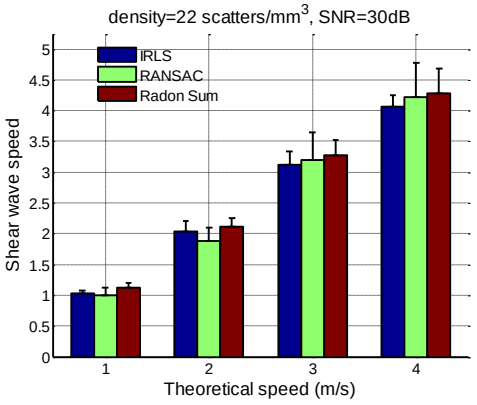

Figure 6. Results with Different Theoretical Speed

5. Conclusion

This paper describes a simulation method to generate the pulse-echo RF signals by Green's function and Field II, calculates the displacement profiles along both lateral and axial direction so as to estimate the corresponding shear wave speed using three different methods, IRLS, RANSAC and Radon Sum. Good agreements are found for these methods in several simulation configurations, different SNR, different scatterer density and different shear wave speed. The values of bias for all the three methods are less than 10%. Compared with Radon Sum and IRLS, it is not so statistical stable for RANSAC, in other words, the standard deviation is greater than the other two methods, because its repeated executions on the same data can yield varying values. Meanwhile, the bias values of Radon Sum are greater than IRLS and RANSAC. IRLS method is suitable for use in real-time situation because of the limited data set and is robust to outliers as RANSAC and Radon Sum. Both its bias and SD are systematically smaller than the other two methods.

Acknowledgments

This work was supported in part by the Foundation of China and Natural Science Foundation of Sichuan Province (Grant No. 2013GZX0147-3).

References

[1] K. J. Parker, M. M. Doyley and D. J. Rubens, "Imaging the elastic properties of tissue: The 20-year perspective", Phys. Med. Biol., vol. 56, **(2011)**, pp. R1–R29.
[2] J. R. Doherty, G. E. Trahey, K. R. Nightingale and M. L. Palmeri, "Acoustic radiation force elasticity imaging in diagnostic ultrasound", IEEE Trans. Ultrason., Ferroelect., Freq. Contr., vol. 60, no. 4, **(2013)**, pp. 685-701.
[3] A. P. Sarvazyan, O. V. Rudenko, S. D. Swanson, J. B. Fowlkes and S. Y. Emelianov, "Shear wave elasticity imaging: A new ultrasonic technology of medical diagnostics", Ultrasound Med. Biol., vol. 24, **(1998)**, pp. 1419–1435.
[4] L. Sandrin, B. Fourquet, J. M. Hasquenoph, S. Yon, C. Fournier, F. Mal, C. Christidis, M. Ziol , B. Poulet, F. Kazemi, M. Beaugrand and R. Palau, "Transient elastography: a new noninvasive method for assessment of hepatic fibrosis", Ultrasound Med. Biol., vol. 29, no. 12, **(2003)**, pp. 1705–1713.
[5] J. McLaughlin and D. Renzi, "Shear wave speed recovery in transient elastography and supersonic imaging using propagating fronts", Inverse Problems, vol. 22, no. 2, **(2006)**, pp. 681–706.
[6] J. Bercoff, M. Tanter, M. Muller and M. Fink, "The role of viscosity in the impulse diffraction field of elastic waves induced by the acoustic radiation force". IEEE Trans. Ultrason., Ferroelect., Freq. Contr., vol. 51 no. 11, **(2004)**, pp. 1523-1536.
[7] M. L. Palmer, S. A. McAleavey, G. E. Trahey and K. R. Nightingale, "Ultrasonic tracking of acoustic radiation force-induced displacements in homogeneous media", IEEE Trans. Ultrason. Ferroelect. Freq. Contr., vol. 53, no. 7, **(2006)**, pp. 1300-1313.
[8] J. A. Jensen, "Field: A Program for Simulating Ultrasound Systems", Medical & Biological Engineering & Computing, vol. 34, no. 1, **(1996)**, pp. 351-353.

[9] H. Hasegawa and H. Kanai, "Improving accuracy in estimation of artery-wall displacement by referring to center frequency of RF echo", IEEE Trans. Ultrason., Ferroelect., Freq. Contr., vol. 53, no. 1, **(2006)**, pp. 52-63.
[10] M. L. Palmeri, M. H. Wang, J. J. Dahl, K. D. Frinkley and K. R. Nightingale, "Quantifying hepatic shear modulus in vivo using acoustic radiation force", Ultrasound Med. Biol. vol. 34, no. 4, **(2008)**, pp. 546–558.4
[11] M. A. Fischler and R. C. Bolles, "Random sample consensus: a paradigm for model fitting with applications to image analysis and automated cartography", Commun. ACM, vol. 24, no. 6, **(1981)**, pp. 381–395.
[12] M. H Wang, M. L. Parlmeri, V. M. Rotemberg, N. C. Rouze and K. R. Nightingale, "Improving the Robustness of Time-of-Flight Based Shear Wave Speed Reconstruction Methods Using RANSAC in Human Liver in vivo", Ultrasound Med. Biol., vol. 36, no. 5, **(2010)**, pp. 802-813.
[13] N. C. Rouze, M. H. Wang, M. L. Palmeri and K. R. Nightingale, "Robust Estimation of Time-of-Flight Shear Wave Speed Using a Radon Sum Transformation", IEEE Trans Ultrason Ferroelectr Freq Control, vol. 57, no. 12, **(2010)**, pp. 2662-2670.
[14] P. W. Holland and R. E. Welsch, "Robust Regression Using Iteratively Reweighted Least-Squares", Communications in Statistics: Theory and Methods, vol. 6, no. 9, **(1977)**, pp. 813-827.